Math Geosci
DOI 10.1007/s11004-017-9677-y

High-Performance Parallel Solver for Integral Equations of Electromagnetics Based on Galerkin Method

Mikhail Kruglyakov[1,2] · **Lidia Bloshanskaya**[3]

Received: 18 December 2015 / Accepted: 25 January 2017

Abstract A new parallel solver for the volumetric integral equations (IE) of electrodynamics is presented. The solver is based on the Galerkin method, which ensures convergent numerical solution. The main features include: (i) memory usage eight times lower compared with analogous IE-based algorithms, without additional restrictions on the background media; (ii) accurate and stable method to compute matrix coefficients corresponding to the IE; and (iii) high degree of parallelism. The solver's computational efficiency is demonstrated on a problem of magnetotelluric sounding of media with large conductivity contrast, revealing good agreement with results obtained using the second-order finite-element method. Due to the effective approach to parallelization and distributed data storage, the program exhibits perfect scalability on different hardware platforms.

Keywords Integral equations · Forward modeling · Electromagnetic sounding · Galerkin method · Green's tensor · High-performance computing

✉ Mikhail Kruglyakov
mkruglyakov@cs.msu.su

Lidia Bloshanskaya
bloshanl@newpaltz.edu

1 Faculty of Computational Mathematics and Cybernetics, Lomonosov MSU, GSP-1, Leninskiye Gory, 1-52, Moscow, Russia 119991

2 Institute of Geophysics, ETH Zurich, Sonneggstrasse 5, 8092 Zurich, Switzerland

3 Department of Mathematics, SUNY New Paltz, 1 Hawk Dr, New Paltz, NY 12561, USA

Published online: 03 March 2017

1 Introduction

Electromagnetic (EM) methods are used in geophysics to model the subsurface electrical conductivity distribution. Conductivity is affected by rock type and composition, temperature, and fluid/melt content and thus can be used in various engineering and industrial problems such as detection of hydrocarbon (low-conductive) and geothermal or ore (high-conductive) reservoirs. Measured electrical and/or magnetic fields are further interpreted via calculations using a given three-dimensional model of the conductivity distribution. Maxwell's equation describing the EM field distribution cannot be solved analytically in the general case, requiring numerical simulation. Large numbers of such simulations are required, and complex large-scale models are invoked (Chave and Jones 2012).

The growing amount of data calls for development of new numerical methods that can deliver fast and accurate EM simulations and harness the computational power provided by modern high-performance multicore and multinode platforms.

There are three basic approaches to numerical simulation of EM fields in conductive media, namely the finite-difference (FD), finite-element (FE), and volumetric integral equation (IE) methods. FD schemes dominated in EM sounding for decades (Egbert and Kelbert 2012; Haber and Ascher 2001; Jaysaval et al. 2015; Mackie et al. 1994; Newman and Alumbaugh 2002). However, FE methods have become popular in recent years (Farquharson and Miensopust 2011; Grayver and Kolev 2015; Puzyrev et al. 2013; Ren et al. 2013; Schwarzbach et al. 2011). IE methods are not so commonly applied, due to certain challenges in their implementation, although their use is described in literature (Avdeev et al. 2002; Hursan and Zhdanov 2002; Kamm and Pedersen 2014; Koyama et al. 2008; Singer 2008).

The main difference between these approaches lies in the discretization outcome. The model usually consists of a number of nonuniform three-dimensional anomalies embedded in one-dimensional (layered) background media. While FD and FE methods produce large sparse systems (Ernst and Gander 2012), the IE method results in compact dense system matrices. This compactness is achieved since the modeling region is confined to the three-dimensional conductivity structures (anomalies) under investigation (Raiche 1974; Weidelt 1975). Note that the boundary conditions are satisfied by construction of Green's functions. By contrast, in FD and FE methods, one has to discretize a volume much larger in both lateral and vertical directions to enable decay (or stabilization) of the EM field at the boundaries of the modeling domain (Grayver and Kolev 2015; Mulder 2006). Another distinction between the methods is the condition number of the matrices (which controls the stability of the solution). In FD and FE methods, the condition number depends on the discretization and frequency, whereas in the IE approach it does not (Pankratov et al. 1995; Singer 1995).

The main focus in the development and implementation of numerical methods for the IE is the efficiency and performance for the large number of unknown parameters. The iterative numerical solver for the IE proposed herein addresses this issue both mathematically (increasing the accuracy and stability of coefficient computations and reducing memory usage) and computationally (allowing high degree of parallelism without memory loss at nodes). A special class of integral equations is used, i.e., those

with a contracting kernel (CIE) (Pankratov et al. 1995; Singer 1995). The CIE were proved to have a unique solution and a well-conditioned (by construction) system matrix (Pankratov et al. 1995; Singer 1995). The Galerkin method is used to solve the CIE numerically (Delves and Mohamed 1985). It has been proved (Kruglyakov 2011; Singer 2008) that the corresponding solution converges.

Two main issues in numerical solution of the IE are the calculation of the matrix coefficients with sufficient accuracy (Wannmaker 1991), and the storage of this dense matrix in some packed form (Avdeev et al. 1997, 2002). The Galerkin method with piecewise-constant basis allows one to address both of these issues; namely, the system matrix is decomposed into sums and products of diagonal and block Toeplitz matrices. First, the matrix coefficients (i.e., double volumetric integrals of the product of basis functions and the CIE kernel) are analytically transformed into one-dimensional convolution integrals. These convolution integrals are then computed using a digital filtering approach. One should bear in mind that only the weights of these filters are computed numerically, whereas the functions in the knots are computed analytically. The resulting system is solved using the flexible generalized minimal residual (GMRES) method (Saad 1993).

The proposed solver exhibits three main features: (1) The memory usage is eight times lower compared with analogous IE-solving algorithms. It is important to stress that memory is saved for any background with arbitrary number of layers. In contrast, in (Kamm and Pedersen 2014), the memory reduction is achieved only in case of a homogeneous half-space background and for uniform vertical discretization, while in (Avdeev and Knizhnik 2009; Koyama et al. 2008; Sun and Kuvshinov 2015), it is achieved at the expense of accuracy and performance. The idea behind the proposed solver is to combine the Galerkin method with the properties of the EM field, namely Lorentz reciprocity. The matrix of the ensuing linear system can be separated into symmetric and antisymmetric submatrices. This reduces the memory requirements by eight times (Sect. 3). (2) Efficient and accurate method for the computation of these matrices (Sect. 3). (3) Implementation with high degree of parallelism. Computational experiments performed with the Bluegene/P and Lomonosov supercomputers at MSU and the high-performance computer (HPC) Piz Daint at the Swiss National Supercomputing Center showed that the solver makes best use of 128–2048 nodes for calculation at a single frequency with a single source. The program exhibits perfect scalability.

This paper is organized as follows: Section 2 is devoted to an overview of the CIE approach and the construction of the approximating system of linear equations. Section 3 addresses the reduction in memory requirements, the computation of matrix coefficients, and features of parallel implementation. In Sect. 4, the computational results for the large (more than 3×10^4) conductivity contrast COMMEMI3D-3 model (Hursan and Zhdanov 2002; Varentsov et al. 2000) are compared with corresponding results obtained using the FE method by (Grayver and Kolev 2015). Appendices A to C provide mathematical details of the presented method.

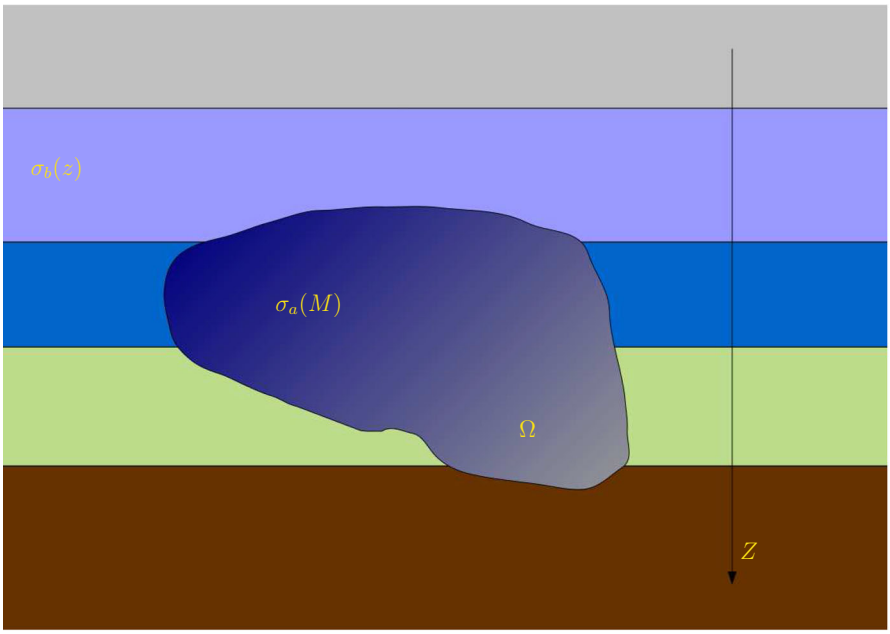

Fig. 1 Typical model

2 Contracting Integral Equation

2.1 Overview

Assume that the EM fields are induced by the external electric currents $\mathbf{J}_{\text{ext}}$. Moreover, assume that the EM fields are time dependent as $e^{-i\omega t}$, where ω is an angular frequency, $i = \sqrt{-1}$, and the magnetic permeability μ_0 is the same in the whole space. Let $\sigma(M)$, $\mathbf{Re}\,\sigma(M) \geq 0$ be a three-dimensional complex conductivity distribution in space. Then, the electrical field $\mathbf{E}$ and the magnetic field $\mathbf{H}$ give the solution of the system of Maxwell's equations

$$\begin{cases} \operatorname{curl} \mathbf{H} = \sigma \mathbf{E} + \mathbf{J}_{\text{ext}}, \\ \operatorname{curl} \mathbf{E} = i\omega\mu_0 \mathbf{H}. \end{cases} \tag{1}$$

The solution of system (1) is unique under the additional radiation conditions at infinity (Ward and Hohmann 1988).

Let $\Omega \subset \mathbf{R}^3$ be some bounded domain and $\sigma(M) = \sigma_b(z)$ for $M(x, y, z) \notin \Omega$ and $\sigma(M) = \sigma_a(M)$ for $M \in \Omega$ (Fig. 1).

Then, for any $M \in \mathbf{R}^3$, the fields $\mathbf{E}(M)$ and $\mathbf{H}(M)$ can be expressed in terms of the integrals

$$\begin{aligned}\mathbf{E}(M) &= \mathbf{E}^{\mathrm{N}}(M) + \int_{\Omega} \widehat{G}^{E}(M, M_0)\,(\sigma_{\mathrm{a}}(M_0) - \sigma_{\mathrm{b}}(M_0))\,\mathbf{E}(M_0)\mathrm{d}\Omega_{M_0},\\ \mathbf{H}(M) &= \mathbf{H}^{\mathrm{N}}(M) + \int_{\Omega} \widehat{G}^{H}(M, M_0)\,(\sigma_{\mathrm{a}}(M_0) - \sigma_{\mathrm{b}}(M_0))\,\mathbf{E}(M_0)\mathrm{d}\Omega_{M_0}.\end{aligned} \tag{2}$$

Here, $\widehat{G}^{E}$ and $\widehat{G}^{H}$ are electrical and magnetic Green's tensors, respectively (Dmitriev et al. 2002; Pankratov et al. 1995). The terms $\mathbf{E}^{\mathrm{N}}$ and $\mathbf{H}^{\mathrm{N}}$ are called the normal electric and magnetic fields, corresponding. They form the solution of the system

$$\begin{cases}\operatorname{curl}\mathbf{H}^{\mathrm{N}} = \sigma_{\mathrm{b}}(z)\mathbf{E}^{\mathrm{N}} + \mathbf{J}_{\mathrm{ext}},\\ \operatorname{curl}\mathbf{E}^{\mathrm{N}} = \mathrm{i}\omega\mu_0\mathbf{H}^{\mathrm{N}},\end{cases} \tag{3}$$

with corresponding conditions at infinity. Note that $\widehat{G}^{E}$ and $\widehat{G}^{H}$ are independent of the anomalous conductivity σ_{a}.

Let $\mathbf{L}_2[\Omega]$ be a Hilbert functional space of vector functions $\mathbf{V}$ with the following norm and dot product:

$$\begin{aligned}(\mathbf{V}, \mathbf{U})_{\mathbf{L}_2[\Omega]} &= \int_{\Omega} \left(V_x(M)\overline{U}_x(M) + V_y(M)\overline{U}_y(M) + V_z(M)\overline{U}_z(M)\right)\mathrm{d}\Omega_M,\\ \|\mathbf{V}\|_{\mathbf{L}_2[\Omega]} &= \sqrt{(\mathbf{V}, \mathbf{V})}.\end{aligned} \tag{4}$$

Suppose $\mathbf{Re}\,\sigma_{\mathrm{b}}(z) > 0$ for $M(x, y, z) \in \Omega$ (the typical EM sounding situation), then the operator $\mathbf{G}^{\mathrm{m}}_{\mathrm{E}}$ is defined as

$$\mathbf{G}^{\mathrm{m}}_{\mathrm{E}}\,\mathbf{V} = \sqrt{\mathbf{Re}\,\sigma_{\mathrm{b}}}\,\widehat{\mathrm{G}}^{\mathrm{E}}\left[2\sqrt{\mathbf{Re}\,\sigma_{\mathrm{b}}}\mathbf{V}\right] + \mathbf{V}, \tag{5}$$

where $\widehat{\mathrm{G}}^{\mathrm{E}}$ is an integral operator from the first equation in relationships (2). The operator $\mathbf{G}^{\mathrm{m}}_{\mathrm{E}}$ is a contracting operator in $\mathbf{L}_2[\Omega]$ (Pankratov et al. 1995; Singer 1995). Using Eqs. (2) and (5), one obtains the CIE for $\mathbf{E}$ as

$$\begin{aligned}&\left(\mathrm{I} - \mathbf{G}^{\mathrm{m}}_{\mathrm{E}}\frac{b}{a}\right)\widetilde{\mathbf{E}} = \sqrt{\mathbf{Re}\,\sigma_{\mathrm{b}}}\mathbf{E}^{\mathrm{N}},\\ &\widetilde{\mathbf{E}} = a\mathbf{E}, \quad a = \frac{\sigma_{\mathrm{a}} + \overline{\sigma_{\mathrm{b}}}}{2\sqrt{\mathbf{Re}\,\sigma_{\mathrm{b}}}}, \quad b = \frac{\sigma_{\mathrm{a}} - \sigma_{\mathrm{b}}}{2\sqrt{\mathbf{Re}\,\sigma_{\mathrm{b}}}},\end{aligned} \tag{6}$$

where I is the identity operator and $\overline{\sigma_{\mathrm{b}}}$ means complex conjugation of σ_{b}.

2.2 Galerkin Method

Suppose that the domain Ω is divided into nonoverlapping subdomains $\Omega = \cup\Omega_n$, $n = 1 \ldots N$ and that $\sigma_{\mathrm{b}}(M) = \sigma^n_{\mathrm{b}}$, $\sigma_{\mathrm{a}}(M) = \sigma^n_{\mathrm{a}}$ for $M \in \Omega_n$, $n = 1 \ldots N$. For each subdomain Ω_n, define the function $W_n(M)$ as

$$W_n(M) = \begin{cases} \dfrac{1}{V_n}, & M \in \Omega_n, \\ 0, & M \notin \Omega_n, \end{cases} \quad V_n = \int\limits_{\Omega_n} \mathrm{d}\Omega_M, \quad n = 1 \ldots N. \tag{7}$$

Let $\widetilde{\mathbf{W}}^N$ be a linear span of the vector functions $\mathbf{W}_n$, $\mathbf{W}_n = (W_{n_x}, W_{n_y}, W_{n_z})$, $n_x, n_y, n_z = 1 \ldots N$ and $\mathbf{P}^{\mathrm{N}}$ be a projection operator from $\mathbf{L}_2[\Omega]$ to $\widetilde{\mathbf{W}}^N$:

$$\forall \mathbf{F} \in \mathbf{L}_2[\Omega] \quad \left[\mathbf{P}^{\mathrm{N}}[\mathbf{F}]\right]_\gamma = \sum_{n=1}^{N} \alpha_n^\gamma W_n, \quad \alpha_n^\gamma = \frac{\int\limits_{\Omega_n} F_\gamma(M)\mathrm{d}\Omega_M}{V_n}, \tag{8}$$

where $\gamma = x, y, z$. Note that $\left\|\mathbf{P}^{\mathrm{N}}\right\| = 1$.

Applying $\mathbf{P}^{\mathrm{N}}$ to the first equation in Eq. (6), one obtains the operator equation in $\widetilde{\mathbf{W}}^N$:

$$\begin{aligned} &\mathbf{W} - \mathbf{P}^{\mathrm{N}}\,\mathbf{G}_{\mathrm{E}}^{\mathrm{m}}\,\frac{b}{a}\mathbf{W} = \mathbf{W}^0, \\ &\mathbf{W}^0 = \mathbf{P}^{\mathrm{N}}\sqrt{\mathbf{Re}\,\sigma_{\mathrm{b}}}\mathbf{E}^{\mathrm{N}}. \end{aligned} \tag{9}$$

Using the definition of $\widetilde{\mathbf{W}}^N$, the components of $\mathbf{W} = (W_x, W_y, W_z)$ can be expressed as

$$W_\gamma = \sum_{k=1}^{N} U_n^\gamma W_n, \quad \gamma = x, y, z. \tag{10}$$

Using Eqs. (8)–(10) and taking into account that σ_{a} and σ_{b} are piecewise functions, one obtains the following system of linear equations for the coefficients $\mathbf{U}_n = (U_n^x, U_n^y, U_n^z)$, $n = 1 \ldots N$:

$$\mathbf{U}_n - \sum_{m=1}^{N} \hat{\gamma}^m \widehat{K}_n^m \mathbf{U}_m = \mathbf{U}_n^0, \tag{11}$$

where

$$\begin{aligned} \widehat{K}_n^m &= \hat{I} + \frac{2}{V_n}\sqrt{\mathbf{Re}\,\sigma_{\mathrm{b}}^m\,\mathbf{Re}\,\sigma_{\mathrm{b}}^n}\,\hat{B}_n^m, \\ \widehat{B}_n^m &= \int\limits_{\Omega_n}\int\limits_{\Omega_m} \widehat{G}^E(M, M_0)\mathrm{d}\Omega_{M_0}\mathrm{d}\Omega_M, \\ \hat{\gamma}^m &= \frac{\sigma_{\mathrm{a}}^m - \sigma_{\mathrm{b}}^m}{\sigma_{\mathrm{a}}^m + \overline{\sigma_{\mathrm{b}}^m}}, \\ \mathbf{U}_n^0 &= \frac{\sqrt{\mathbf{Re}\,\sigma_{\mathrm{b}}^n}}{V_n}\int\limits_{\Omega_n} \mathbf{E}^{\mathrm{N}}(M)\mathrm{d}\Omega_M. \end{aligned} \tag{12}$$

Note that $\widehat{K}_n^m$, $\widehat{B}_n^m$, $\hat{I}$, and $\hat{\gamma}^m$ are 3×3 matrices with $\hat{I}$ being an identity matrix and $\hat{\gamma}^m$ a diagonal matrix. The system (11) has a unique solution (Kruglyakov 2011; Singer 2008).

Using the solution $\mathbf{U}_n$ of system (11), one can approximate $\widetilde{\mathbf{E}}(M)$ and $\widetilde{\mathbf{H}}(M)$ for any point $M \in R^3$ with

$$\begin{aligned}\mathbf{E}(M) \approx \widetilde{\mathbf{E}}(M) &= \mathbf{E}^{\mathrm{N}}(M) + \sum_{n=1}^{N} \left(\sigma_{\mathrm{a}}^n - \sigma_{\mathrm{b}}^n\right) \mathbf{U}_n \int\limits_{\Omega_n} \widehat{G}^E(M, M_0)\mathrm{d}\Omega_{M_0}, \\ \mathbf{H}(M) \approx \widetilde{\mathbf{H}}(M) &= \mathbf{E}^{H}(M) + \sum_{n=1}^{N} \left(\sigma_{\mathrm{a}}^n - \sigma_{\mathrm{b}}^n\right) \mathbf{U}_n \int\limits_{\Omega_n} \widehat{G}^H(M, M_0)\mathrm{d}\Omega_{M_0}.\end{aligned} \tag{13}$$

Relations (13) are first-order approximations of d in $\mathbf{C}$ for $M \notin \Omega$ (Kruglyakov 2011), and result in fast and relatively simple computations. The main challenge is to calculate the matrix coefficients and solve the system (11).

3 Computational Challenges

3.1 Memory Requirements

The main challenge of the integral equation approach is to solve the system of linear equations with dense matrices (Eq. 11). Storage of these matrices in RAM is also problematic. The standard approach (Avdeev et al. 1997) is to use the property

$$\widehat{G}^E(M, M_0) = \widehat{G}^E(x - x_0, y - y_0, z, z_0). \tag{14}$$

For implementation purposes, consider now $\Omega \subset R^3$ to be a rectangular domain. As before, Ω is divided into $N = N_x N_y N_z$ rectangular subdomains Ω_n, $n = 1, \ldots, N$, where N_x, N_y, N_z are the number of subdomains in X, Y, Z direction, respectively. Suppose also that each Ω_n has the same size $h_x \times h_y$ in the XY plane. Then,

$$\widehat{B}_n^m = \int\limits_{\Omega_n}\int\limits_{\Omega_m} \widehat{G}^E(M, M_0)\mathrm{d}\Omega_{M_0}\mathrm{d}\Omega_M = \widehat{B}_n^m\left(I_x^n - I_x^m, I_y^n - I_y^m, I_z^n, I_z^m\right), \tag{15}$$

where $I_x^n, I_x^m \in \{1, 2, \ldots N_x\}$, $I_y^n, I_y^m \in \{1, 2, \ldots N_y\}$, $I_z^n, I_z^m \in \{1, 2, \ldots N_z\}$, $n, m = 1 \ldots N$. Therefore, $\widehat{B}_n^m$ is a block Toeplitz matrix induced by the block vector $(C^y_{-(N_y-1)}, C^y_{-(N_y-2)}, \ldots, C^y_{N_y-2}, C^y_{N_y-1})$. Each block $C_i^y, i = -(N_y - 1) \ldots N_y - 1$ is also a block Toeplitz matrix and is induced by the block vector $(D^i_{-(N_x-1)}, D^i_{-(N_x-2)}, \ldots D^i_{N_x-2}, D^i_{N_x-1})$. D^i_j is a 3×3 block matrix with the structure

$$D^i_j = Q(i, j) = \begin{pmatrix} Q_{xx} & Q_{xy} & Q_{xz} \\ Q_{yx} & Q_{yy} & Q_{yz} \\ Q_{zx} & Q_{zy} & Q_{zz} \end{pmatrix}. \tag{16}$$

Here, $Q_{\alpha\beta}$ are matrices of order N_z, $\alpha, \beta = x, y, z$, $i = -(N_y - 1) \ldots N_y - 1$, $j = -(N_x - 1) \ldots N_x - 1$.

Let A be a matrix corresponding to the system of linear Eq. (11). Then,

$$A = S + R_1 B R_2, \tag{17}$$

where S, R_1, and R_2 are diagonal matrices; $B = \left\{\widehat{B}_n^m\right\}$ is the block Toeplitz matrix described above.

In view of Eq. (17), it follows that only $36 \cdot N_x N_y N_z^2 \cdot 16 + O(N_x N_y N_z)$ bytes are required to store matrix A in double precision. Using the equivalence $G_{xy}^E = G_{yx}^E$, this requirement can be reduced to $32 \cdot N_x N_y N_z^2 \cdot 16 + O(N_x N_y N_z)$ bytes, as in (Avdeev et al. 1997). This memory requirement can be reduced eight times by virtue of the following lemmas:

Lemma 1 *If $\widehat{G}^E(M, M_0)$ is an electrical Green's tensor of any layered media, then it possesses the following symmetric and antisymmetric properties in Cartesian coordinates along the vertical dimension:*

$$\begin{aligned}
G_{xx}^E(x - x_0, y - y_0, z, z_0) &= G_{xx}^E(x - x_0, y - y_0, z_0, z),\\
G_{yy}^E(x - x_0, y - y_0, z, z_0) &= G_{yy}^E(x - x_0, y - y_0, z_0, z),\\
G_{zz}^E(x - x_0, y - y_0, z, z_0) &= G_{zz}^E(x - x_0, y - y_0, z_0, z),\\
G_{xy}^E(x - x_0, y - y_0, z, z_0) &= G_{yx}^E(x - x_0, y - y_0, z, z_0),\\
G_{xy}^E(x - x_0, y - y_0, z, z_0) &= G_{xy}^E(x - x_0, y - y_0, z_0, z),\\
G_{zx}^E(x - x_0, y - y_0, z, z_0) &= -G_{xz}^E(x - x_0, y - y_0, z_0, z),\\
G_{zy}^E(x - x_0, y - y_0, z, z_0) &= -G_{yz}^E(x - x_0, y - y_0, z_0, z).
\end{aligned} \tag{18}$$

Lemma 2 *If $\widehat{G}^E(M, M_0)$ is an electrical Green's tensor of any layered media, then it possesses the following symmetric and antisymmetric properties in Cartesian coordinates along the lateral dimensions:*

$$\begin{aligned}
G_{\alpha\alpha}^E(x - x_0, y - y_0, z, z_0) &= G_{\alpha\alpha}^E(x_0 - x, y - y_0, z, z_0) =\\
G_{\alpha\alpha}^E(x - x_0, y_0 - y, z, z_0) &= G_{\alpha\alpha}^E(x_0 - x, y_0 - y, z, z_0),\\
G_{xy}^E(x - x_0, y - y_0, z, z_0) &= -G_{xy}^E(x_0 - x, y - y_0, z, z_0) =\\
-G_{xy}^E(x - x_0, y_0 - y, z, z_0) &= G_{xy}^E(x_0 - x, y_0 - y, z, z_0),\\
G_{zx}^E(x - x_0, y - y_0, z, z_0) &= -G_{zx}^E(x_0 - x, y - y_0, z, z_0) =\\
G_{zx}^E(x - x_0, y_0 - y, z, z_0) &= -G_{zx}^E(x_0 - x, y_0 - y, z, z_0),\\
G_{zy}^E(x - x_0, y - y_0, z, z_0) &= G_{zy}^E(x_0 - x, y - y_0, z, z_0) =\\
-G_{zy}^E(x - x_0, y_0 - y, z, z_0) &= -G_{zy}^E(x_0 - x, y_0 - y, z, z_0),\\
\alpha &\in \{x, y, z\}.
\end{aligned} \tag{19}$$

These lemmas are trivial corollaries from Lorentz reciprocity (Ward and Hohmann 1988) and formulas for the Green's tensor components (see Appendix A). Relations (15) and (18) give

$$
\begin{aligned}
&Q_{zx} = -Q_{xz}^{\mathrm{T}},\ Q_{zy} = -Q_{yz}^{\mathrm{T}},\\
&Q_{xx} = Q_{xx}^{\mathrm{T}},\ Q_{yy} = Q_{yy}^{\mathrm{T}},\ Q_{zz} = Q_{zz}^{\mathrm{T}},\\
&Q_{xy} = Q_{xy}^{\mathrm{T}} = Q_{yx} = Q_{yx}^{\mathrm{T}},
\end{aligned}
\tag{20}
$$

where superscript "T" indicates matrix transpose.

Therefore, one needs to store only Q_{xz}, Q_{yz} and the upper diagonal parts of Q_{xx}, Q_{xy}, Q_{yy}, Q_{zz}. Moreover, the values $Q(i, j)$ can be stored for only $i = 0, \ldots, N_y - 1$, $j = 0, \ldots, N_x - 1$, since Eq. (19) allows one to obtain these values for negative i or j from suitable symmetric/antisymmetric properties.

Thus, only $2 \cdot N_x N_y N_z \cdot (2N_z + 1) \cdot 16$ bytes are required to store $\widehat{B}_n^m$, which is eight times less than the memory requirements in (Avdeev et al. 1997, 2002; Hursan and Zhdanov 2002). It is worth stressing again that this is valid for any background layered media and without requiring the subdomains to be of the same vertical size.

3.2 Matrix Coefficients Computation

The next computational challenge of the Galerkin approach is evaluation of the coefficients $\widehat{B}_n^m$, $n, m = 1 \ldots N$, i.e., the double volumetric integrals of $\widehat{G}^E$ in the RHS of Eq. (15), with desired accuracy. The components of $\widehat{G}^E$ are improper integrals containing Bessel functions (Appendix A). The integration in vertical direction is performed analytically using the fundamental function of the layered media approach from (Dmitriev et al. 2002), as shown in Appendix B. The main problem, however, is the integration over the horizontal domains. In this case, one needs to compute fifth-order integrals over fast-oscillating functions.

The integrals in Eq. (15) are double volumetric, thus they have only weak singularity. Therefore, one can change the order of integration and make an appropriate substitution to convert the fifth-order integral into a convolution with a specific kernel. Following the standard approach of convolution calculation, the spectrum of this kernel is computed and the digital filter constructed, as shown in Appendix C.

It is important to emphasize that both the knots and the weights in the obtained filter significantly depend on the integration domains. On the contrary, the integration over different horizontal domains is completely data independent. This is used in the parallel algorithm. Computational experiments (Sect. 4) demonstrated that the used filters provide suitable accuracy even for models with large conductivity contrast.

3.3 Parallel Implementation

The most essential part of any iterative method for solving a system of linear equations is the matrix–vector multiplication. Since matrix B is block Toeplitz, one can use the two-dimensional fast Fourier transform (FFT) to speed up this operation (Avdeev et al. 1997). Therefore, instead of matrices $Q(i, j)$, their discrete Fourier transforms $\widetilde{Q}(i, j)$ are stored. This requires the same amount of memory, since the discrete Fourier transform preserves the symmetric/antisymmetric properties of the data.

Table 1 Matrix storage organization

Node 0	...	Node $N_y - 1$	Node N_y	...	Node $2N_y - 1$
$\widetilde{Q}(0, 0)$	...	$\widetilde{Q}(N_y - 1, 0)$	$\widetilde{Q}(0, N_x/2)$	...	$\widetilde{Q}(N_y - 1, N_x/2)$
$\widetilde{Q}(0, 1)$	...	$\widetilde{Q}(N_y - 1, 1)$	$\widetilde{Q}(0, N_x/2 + 1)$	...	$\widetilde{Q}(N_y - 1, N_x/2 + 1)$
$\vdots$	...	$\vdots$	$\vdots$	...	$\vdots$
$\widetilde{Q}(0, N_x/2 - 1)$	...	$\widetilde{Q}(N_y - 1, N_x - 1)$	$\widetilde{Q}(0, N_x - 1)$	...	$\widetilde{Q}(N_y - 1, N_x - 1)$

The multiplication of block Toeplitz matrix B on some vector $\mathbf{V} \in \widetilde{\mathbf{W}}^N$ is performed via the following three-step algorithm:

1. Compute $3N_z$ forward FFT of vector $\mathbf{V}$;
2. Compute $36N_xN_y$ algebraic matrix–vector multiplications of order N_z to obtain vector $\tilde{\mathbf{V}}$;
3. Compute $3N_z$ backward FFT of vector $\tilde{\mathbf{V}}$.

The multiplications in step 2 are further divided into $4N_xN_y$ groups which are mutually data independent. This allows implementation of a special scheme for distributed data storage and a parallel algorithm for the IE solver, as described below.

For simplicity, consider $2N_y$ nodes and assume that N_x is even. The distributed matrix storage is organized in a special way: the half of block vector $\widetilde{Q}(n, j)$, $j = 0 \ldots N_x/2 - 1$ is stored at the nth node $n = 0 \ldots N_y - 1$, while $\widetilde{Q}(n, j)$, $j = N_x/2 \ldots N_x$ is stored at node $n + N_y$, $n = 0 \ldots N_y - 1$ (Table 1).
This storage organization is used to develop a solver with suitable parallelization features:

1. The coefficients of matrices B, S, R_1, R_2 stored at different nodes are computed simultaneously and completely data independently;
2. The iterative method is executed using the authors' distributed implementation of FGMRES (Saad 1993), inspired by (Fraysse et al. 2003);
3. The distributed two-dimensional Fourier transform is computed via the authors' implementation using the FFTW3 library (Frigo and Johnson 2005) for local FFT;
4. The calculation of the local algebraic matrix–vector multiplication is processed using the OpenBLAS library (Wang et al. 2013);
5. For all stages of the computational process, the hybrid MPI+OpenMP scheme is used.

To demonstrate the scalability of the implemented parallelization, the COMMEMI3D-3 model was used with $N_x = 176$, $N_y = 224$, $N_z = 118$, i.e., with cubic subdomains with 25 m edges (Sect. 4). Computational experiments performed at Bluegene/P, HPC Lomonosov (MSU), and Piz Daint (Swiss National Supercomputing Center) showed good speed increment depending on the number of processes (Fig. 2). Matrix calculation time includes the time for the FFT calculation of $\widehat{B}_n^m$. The solid black line means ideal linear speedup. Note that, for such a high-contrast model, the matrix calculation time (crosses) is small enough compared with solving the system of linear equations (circles). One can see that the scalability is close to linear.

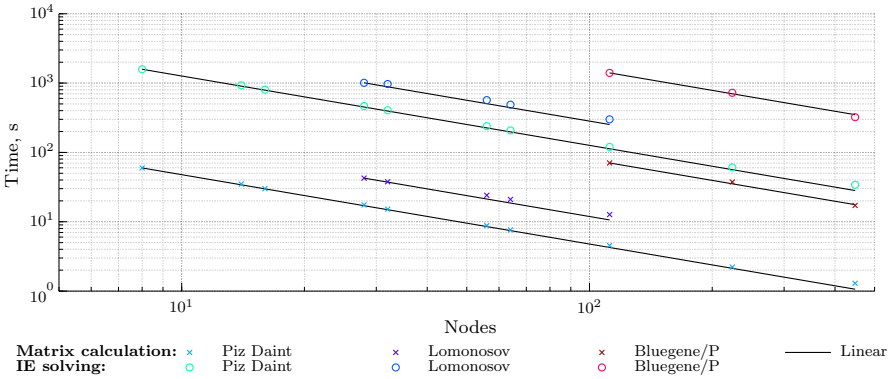

Fig. 2 Strong scalability for COMMEMI3D-3 model

4 Large Conductivity Contrast Modeling

Accurate computation of the EM field for media with high conductivity contrast is one of the most complex problems in EM modeling, due to the strong codependency between the conductivity contrast and matrix condition number (Pankratov et al. 1995; Pankratov and Kuvshinov 2016; Singer 1995). The conductivity contrast is the ratio between the real parts of the anomalous conductivity $\mathbf{Re}\,\sigma_{\mathrm{a}}(M)$ and background conductivity $\mathbf{Re}\,\sigma_{\mathrm{b}}(M)$ at the same point M.

The large conductivity contrast COMMEMI3D-3 model (Hursan and Zhdanov 2002; Varentsov et al. 2000) is used as one of the test models for the presented solver. This model schematically describes a conductivity distribution typical for ore exploration by audio-magnetotelluric sounding. Following magnetotelluric (i.e., low-frequency) sounding tradition, in the rest of this section the conductivity is a real-valued function.

The COMMEMI3D-3 model consists of seven rectangular blocks placed in layered media and oriented along coordinate axes. Their conductivities σ (in S/m) and positions (coordinates of the opposite corners in km) are listed in Table 2 and depicted in Fig. 3. The layered background of the model consists of the upper halfspace $z < 0$ (air) with conductivity of 0 S/m, two layers with conductivity of 10^{-3}, 10^{-4} S/m, and a lower halfspace with conductivity of 0.1 S/m. The thickness of the first and second layers is 1 and 6.5 km, respectively. One can see that the maximum conductivity contrast is 10^4 in the first layer and $3.3 \cdot 10^4$ in the second.

Modeling of magnetotelluric sounding was performed for various discretizations (cubic subdomains of different sizes) and periods $T = 2\pi/\omega$, then compared with results obtained using a modern FE solver (Grayver and Kolev 2015). Figures 4 and 5 present, correspondingly, the apparent resistivity ρ_{xy} at profile $x = 1.9$ km and ρ_{yx} at profile $y = 3.83$ km for the period 1 s. One can see that the agreement with FE (magenta circles) is good even for rather coarse anomaly discretization (black curve). The exception is the area $[3.5, 4.5]$ km on the profile $y = 3.83$ km (Fig. 5) above the high-conductivity block. This is amended by taking finer discretization (azure curve).

Table 2 Coordinates of opposite corners (x_1, y_1, z_1), (x_2, y_2, z_2) in km and conductivities σ (S/m) of COMMEMI3D-3 blocks

	x_1	y_1	z_1	x_2	y_2	z_2	σ
1	0	2.4	0.05	3	2.8	0.3	0.0033
2	0	1.8	0.05	3	2.4	0.45	0.033
3	0	1.4	0.05	3	1.8	0.30	0.1
4	0	0.8	0.05	3	1.4	0.45	0.033
5	0	0.4	0.05	3	0.8	0.30	0.0033
6	3.4	2.8	0.2	4.4	4.8	1	10
7	1.4	0	1	2.4	5.6	3	3.3333

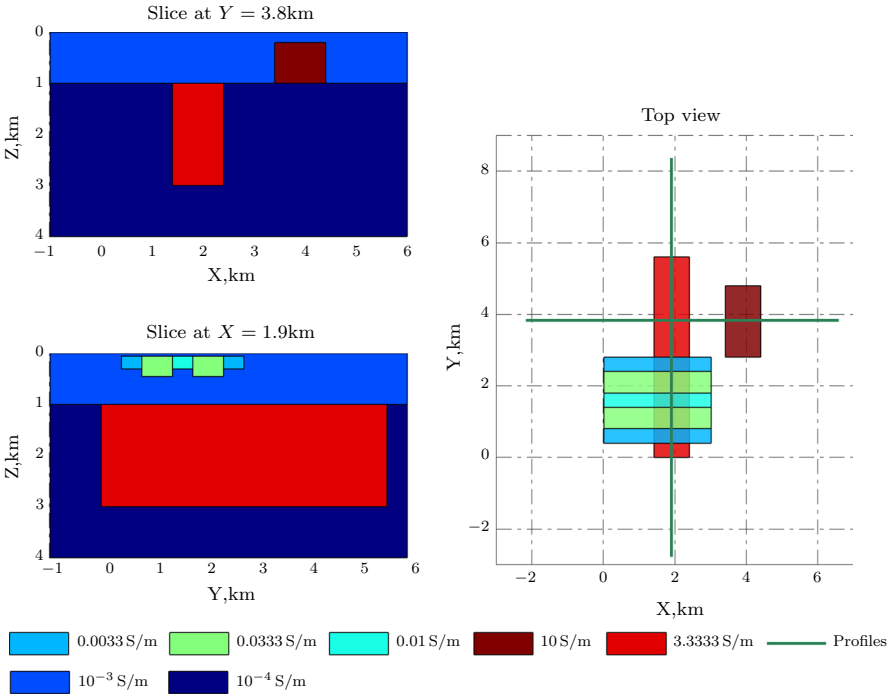

Fig. 3 COMMEMI3D-3 model

Figure 6 shows the apparent conductivity ρ_{yx} at site (3.975, 3.83) km, i.e., above the high-conductivity block, for different periods. One can see that the finer discretization is needed only for the periods $\left[10^{-1}, 10^{1}\right]$ s. The reason behind this effect is the drastic change in the electric field inside the compact high-conductivity block, which does not allow one to use the piecewise approximation on coarse discretization. The compared solver (Grayver and Kolev 2015) uses second-order polynomials, which are very effective in such situations. At the same time, coarse discretization can be efficiently used for smaller and larger periods. It is worth emphasizing that this concerns only the area above the high-conductivity block, while at the point (1.9, 1.7) km, Fig. 7 shows good correspondence for all periods.

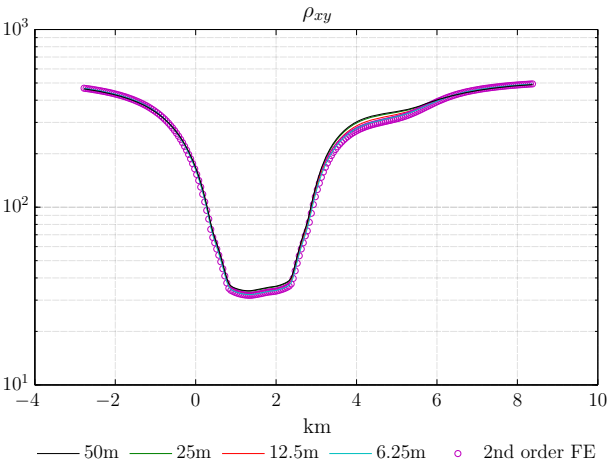

Fig. 4 Apparent resistivity ρ_{xy} at period 1 s along profile $x = 1.9$ km for different subdomain sizes

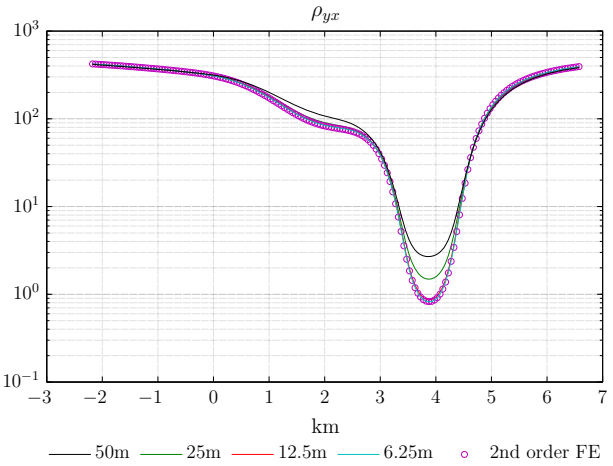

Fig. 5 Apparent resistivity ρ_{yx} at period 1 s along profile $y = 3.83$ km for different subdomain sizes

Figures 8, 9, 10, and 11 demonstrate area distributions of the apparent conductivity and impedance phases for 1 s period. One can see that the variation in apparent conductivity is four orders of magnitude with very drastic transition. The phase change of the impedance is 10°, and the transition is again drastic. It is worth remembering that one of the peculiarities of the IE method is the quite weak dependence of the computational cost on the number of sites where the field is computed. This allows one to obtain maps with such drastic transitions without additional computational cost.

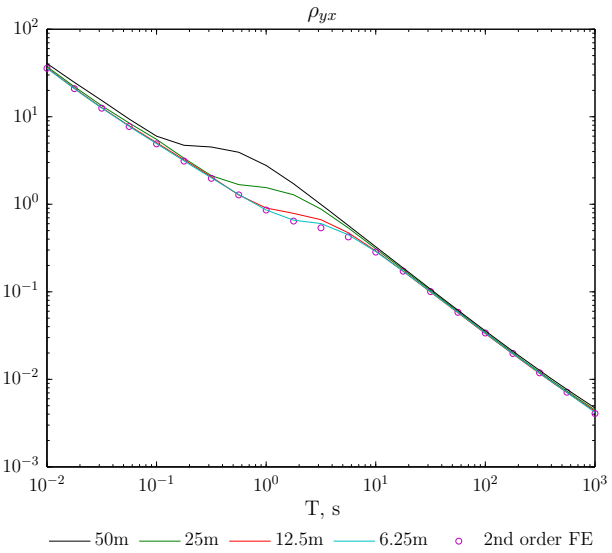

Fig. 6 Apparent resistivity ρ_{yx} at site $x = 3.975\,\text{km}$, $y = 3.83\,\text{km}$ depending on period

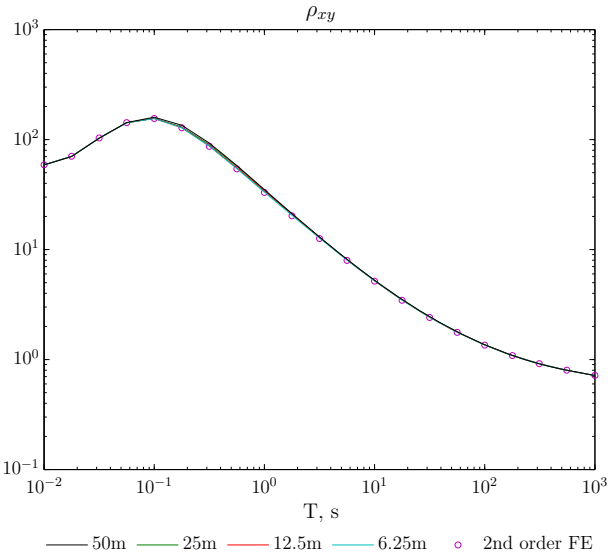

Fig. 7 Apparent resistivity ρ_{xy} at site $x = 1.9\,\text{km}$, $y = 1.7\,\text{km}$ depending on period

5 Conclusions

The presented solver, named the "Gnu Integral Equation Modeling in ElectroMagnetic Geophysics" (GIEM2G), shows impressive performance in terms of both memory requirements and accuracy. The memory requirements are eight times lower compared

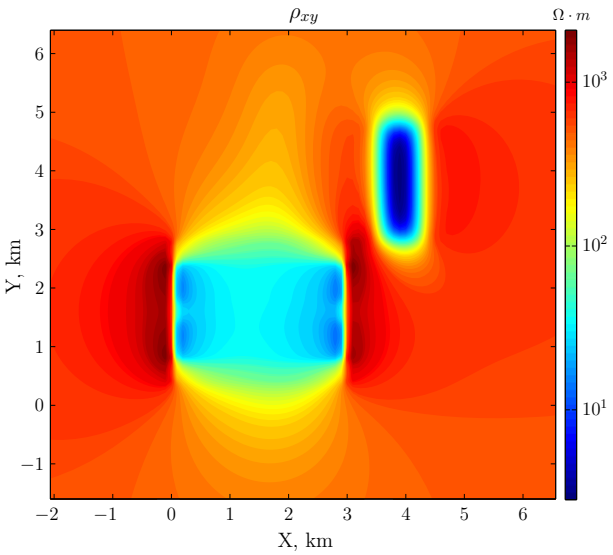

Fig. 8 Apparent resistivity ρ_{xy} at 1 s

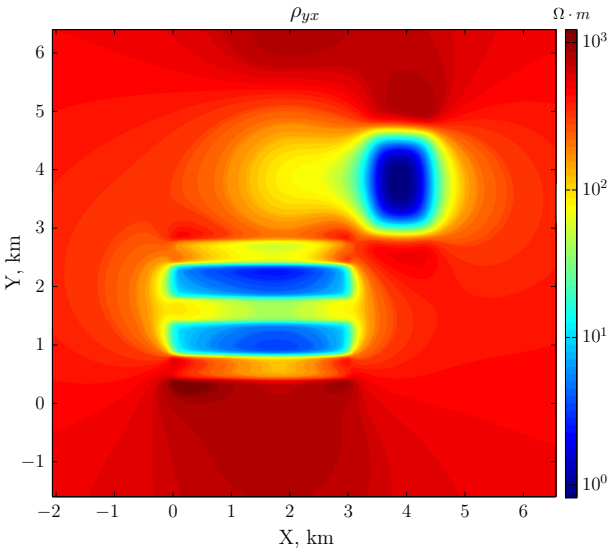

Fig. 9 Apparent resistivity ρ_{yx} at 1 s

with other volumetric IE solvers (Avdeev et al. 1997; Hursan and Zhdanov 2002). This is achieved for any layered background and nonuniform discretization in vertical direction. In this way, average-scale modeling (up to $3 \cdot 10^6$ subdomains) can be efficiently done using laptops, while the parallelization scheme allows use of HPC with hundreds or thousands of nodes for large-scale modeling (up to 10^9 subdomains).

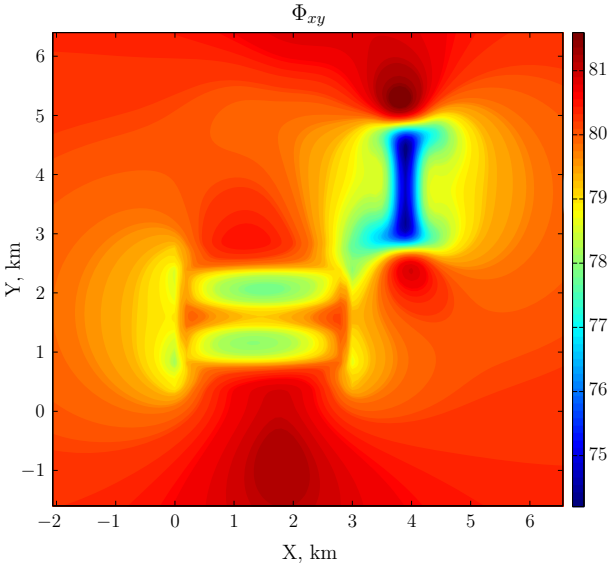

Fig. 10 Impedance phase Φ_{xy} at 1 s

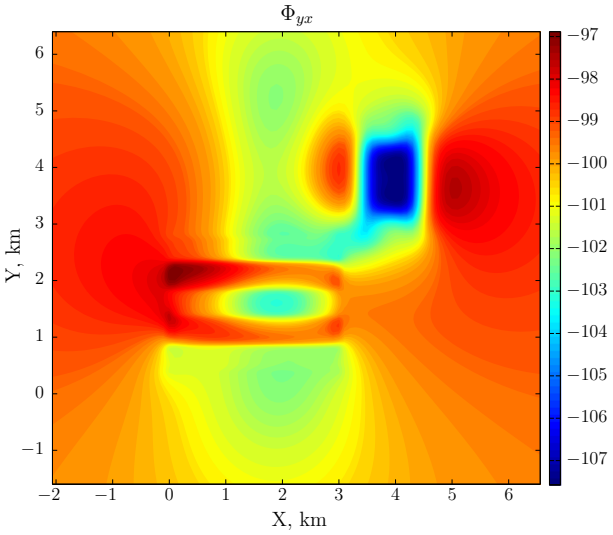

Fig. 11 Impedance phase Φ_{yx} at 1 s

The computational efficiency of the method was demonstrated on the large conductivity contrast ($3.3 \cdot 10^4$) COMMEMI3D-3 model. To the best of the authors' knowledge, this is the first time that comparable results have been achieved for such a high-contrast complex model using different methods (FE and IE). In addition to efficient usage of HPC, the proposed IE method relies on a new technique to calculate the matrix coefficients, based on analytical integration in vertical direction with

a completely new scheme to compute the integrals in horizontal direction. It is worth mentioning that the proposed scheme for the analytical integration is robust in terms of machine precision and needs only $O(N_z)$ computations of complex exponents.

GIEM2G is implemented as hybrid MPI+OpenMP software in modern Fortran language. It is open-source software distributed under the GPLv2 license and can be simply cloned from GitLab by `git -clone git@gitlab.com:m.kruglyakov/GIEM2G.git`. It is also used as an optional computational engine in the forward solver extrEMe (Kruglyakov et al. 2016a) and inverse solver extrEMe-I (Kruglyakov et al. 2016b).

Acknowledgements The research of the first author was supported by the Russian Foundation for Basic Research (grant no. 13-05-12018-OFI_M). As a visiting fellow in ETH Zurich, he was also partially supported by the Swiss National Science Foundation (grant no. IZK0Z2_163494) and ETH Zurich. Authors acknowledge the teams of HPC CMC Lomonosov MSU for access to Bluegene/P HPC, the Lomonosov MSU Research Computing Center for access to HPC Lomonosov (Sadovnichy et al. 2013), and the Swiss National Supercomputing Center (CSCS) grant (project ID s660). The authors would also like to thank Alexander Grayver, ETH Zurich, for providing data for comparison, and Alexey Kuvshinov, ETH Zurich, for suggestions and helpful discussions.

Appendix A: Green's Tensor

Following the notations from (Dmitriev et al. 2002), the electrical $\widehat{G}^E$ and magnetic $\widehat{G}^H$ tensors of layered media can be written as

$$\begin{aligned} \widehat{G}^E &= \widehat{G} + \operatorname{grad}\left(\frac{\mu_0}{k^2}\operatorname{div}\frac{\widehat{G}}{\mu_0}\right), \\ \widehat{G}^H &= \frac{1}{\mathrm{i}\omega\mu_0}\operatorname{curl}\widehat{G}, \\ k^2 &= \mathrm{i}\omega\mu_0\sigma_\mathrm{b}, \end{aligned} \tag{21}$$

where

$$\widehat{G}(M, M_0) = \begin{pmatrix} G_1(M, M_0) & 0 & 0 \\ 0 & G_1(M, M_0) & 0 \\ \frac{\partial g(M,M_0)}{\partial x} & \frac{\partial g(M,M_0)}{\partial y} & G_2(M, M_0) \end{pmatrix} \tag{22}$$

and

$$G_1(M, M_0) = \frac{\mathrm{i}\omega\mu_0}{4\pi}\int_0^\infty J_0(\lambda\rho)U_1(\lambda, z, z_0)\lambda\mathrm{d}\lambda,$$

$$G_2(M, M_0) = \frac{\mathrm{i}\omega\mu_0}{4\pi}\int_0^\infty J_0(\lambda\rho)U_\sigma(\lambda, z, z_0)\lambda\mathrm{d}\lambda,$$

$$g(M, M_0) = -\frac{\mathrm{i}\omega\mu_0}{4\pi}\int_0^\infty J_0(\lambda\rho)\left(\frac{\partial}{\partial z_0}U_\sigma(\lambda, z, z_0) + \frac{\partial}{\partial z}U_1(\lambda, z, z_0)\right)\frac{\mathrm{d}\lambda}{\lambda},$$

$$M = M(x, y, z) \quad M_0 = M_0(x_0, y_0, z_0), \quad \rho = \sqrt{(x - x_0)^2 + (y - y_0)^2}. \tag{23}$$

Here, J_0 is a zero-order Bessel function of the first kind, and functions $U_\gamma(\lambda, z, z_0)$, $\gamma = 1, \sigma$ are the fundamental functions of the layered media (Appendix B).

From Eqs. (21) and (22), one gets

$$\widehat{G}^E = \begin{Bmatrix} G_1 + \frac{1}{k^2}\frac{\partial^2}{\partial x^2}\left(G_1 + \frac{\partial g}{\partial z}\right) & \frac{1}{k^2}\frac{\partial^2}{\partial x \partial y}\left(G_1 + \frac{\partial g}{\partial z}\right) & \frac{1}{k^2}\frac{\partial^2 G_2}{\partial x \partial z} \\ \frac{1}{k^2}\frac{\partial^2}{\partial x \partial y}\left(G_1 + \frac{\partial g}{\partial z}\right) & G_1 + \frac{1}{k^2}\frac{\partial^2}{\partial y^2}\left(G_1 + \frac{\partial g}{\partial z}\right) & \frac{1}{k^2}\frac{\partial^2 G_2}{\partial y \partial z} \\ \frac{\partial g}{\partial x} + \frac{1}{k^2}\frac{\partial^2}{\partial x \partial z}\left(G_1 + \frac{\partial g}{\partial z}\right) & \frac{\partial g}{\partial y} + \frac{1}{k^2}\frac{\partial^2}{\partial y \partial z}\left(G_1 + \frac{\partial g}{\partial z}\right) & G_2 + \frac{1}{k^2}\frac{\partial^2 G_2}{\partial z^2} \end{Bmatrix}. \tag{24}$$

Note that $G^E_{xz}(M, M_0) = -G^E_{zx}(M_0, M)$ and $G^E_{yz}(M, M_0) = -G^E_{zy}(M_0, M)$, according to Lorentz reciprocity.

Let $\Omega_n = S_n \times [z_n^1, z_n^2]$, $\Omega_m = S_m \times [z_m^1, z_m^2]$, where S_n, S_m are horizontal rectangular domains, and let $\sigma_\mathrm{b} = \sigma_\mathrm{b}^n$ inside $[z_n^1, z_n^2]$, $\sigma_\mathrm{b} = \sigma_\mathrm{b}^m$ inside $[z_m^1, z_m^2]$; That is, the subdomains do not intersect the boundaries of the layers. Taking into account Eqs. (12), (21), and (24), one can see that $\widehat{B}_n^m$ is expressed in terms of double volumetric integrals with weak integrable singularity, so the order of integration can be changed. Then, using Eqs. (23) and (24), one obtains

$$\widehat{B}_n^m = \frac{1}{4\pi}\begin{Bmatrix} I_1^{n,m} + I_{xx}^{n,m} & I_{xy}^{n,m} & I_x^{n,m} \\ I_{xy}^{n,m} & I_1^{n,m} + I_{yy}^{n,m} & I_y^{n,m} \\ -I_x^{m,n} & -I_y^{m,n} & I_2^{n,m} + I_{zz}^{n,m} \end{Bmatrix}, \tag{25}$$

where

$$\begin{aligned}
I_1^{n,m} &= \int_{S_n}\int_{S_m}\left(\int_0^\infty J_0(\lambda\rho) V_1^{n,m}(\lambda)\lambda \mathrm{d}\lambda\right)\mathrm{d}x_0\mathrm{d}y_0\mathrm{d}x\mathrm{d}y, \\
I_2^{n,m} &= \int_{S_n}\int_{S_m}\left(\int_0^\infty J_0(\lambda\rho) V_2^{n,m}(\lambda)\lambda \mathrm{d}\lambda\right)\mathrm{d}x_0\mathrm{d}y_0\mathrm{d}x\mathrm{d}y, \\
I_{\alpha\beta}^{n,m} &= \int_{S_n}\frac{\partial^2}{\partial\alpha\partial\beta}\left\{\int_{S_m}\left(\int_0^\infty J_0(\lambda\rho)\left[V_1^{n,m}(\lambda) + V_3^{n,m}(\lambda)\right]\frac{\mathrm{d}\lambda}{\lambda}\right)\mathrm{d}x_0\mathrm{d}y_0\right\}\mathrm{d}x\mathrm{d}y, \\
I_\alpha^{n,m} &= \int_{S_n}\frac{\partial}{\partial\alpha}\left\{\int_{S_m}\left(\int_0^\infty J_0(\lambda\rho) V_4^{n,m}(\lambda)\lambda \mathrm{d}\lambda\right)\mathrm{d}x_0\mathrm{d}y_0\right\}\mathrm{d}x\mathrm{d}y, \\
I_{zz}^{n,m} &= \int_{S_n}\int_{S_m}\left(\int_0^\infty J_0(\lambda\rho) V_5^{n,m}(\lambda)\lambda \mathrm{d}\lambda\right)\mathrm{d}x_0\mathrm{d}y_0\mathrm{d}x\mathrm{d}y.
\end{aligned} \tag{26}$$

Here $\alpha = x, y$, $\beta = x, y$, and

$$V_1^{n,m}(\lambda) = \mathrm{i}\omega\mu_0 \int_{z_n^1}^{z_n^2}\int_{z_m^1}^{z_m^2} U_1(\lambda, z, z_*)\mathrm{d}z_*\mathrm{d}z,$$

$$V_2^{n,m}(\lambda) = \mathrm{i}\omega\mu_0 \int_{z_n^1}^{z_n^2}\int_{z_m^1}^{z_m^2} U_\sigma(\lambda, z, z_*)\mathrm{d}z_*\mathrm{d}z,$$

$$V_3^{n,m}(\lambda) = -\frac{1}{\sigma_\mathrm{b}^n}\int_{z_n^1}^{z_n^2}\frac{\partial}{\partial z}\left(\int_{z_m^1}^{z_m^2}\left[\frac{\partial}{\partial z_*}U_\sigma(\lambda, z, z_*)\right]\mathrm{d}z_*\right)\mathrm{d}z,$$

$$V_4^{n,m}(\lambda) = \frac{1}{\sigma_\mathrm{b}^n}\int_{z_n^1}^{z_n^2}\frac{\partial}{\partial z}\left(\int_{z_m^1}^{z_m^2} U_\sigma(\lambda, z, z_*)\mathrm{d}z_*\right)\mathrm{d}z,$$

$$V_5^{n,m}(\lambda) = \frac{1}{\sigma_\mathrm{b}^n}\int_{z_n^1}^{z_n^2}\frac{\partial^2}{\partial z^2}\left(\int_{z_m^1}^{z_m^2} U_\sigma(\lambda, z, z_*)\mathrm{d}z_*\right)\mathrm{d}z. \tag{27}$$

Therefore, to obtain the coefficients of $\hat{B}_n^m$, one needs computational methods to find "horizontal" integrals (26) and "vertical" integrals (27). These methods are presented in the following appendices.

Appendix B: Vertical Integration

The integrals in formulas (27) are expressed in terms of the so-called fundamental function of layered media (Dmitriev et al. 2002). Consider media with $N_\mathrm{lay} - 1$ homogeneous layers with complex conductivities σ_n, $n = 1 \ldots N_\mathrm{lay} - 1$, the upper halfspace (air, the zeroth layer) with complex conductivity σ_0, and the lower halfspace (the N_lay-th layer) with conductivity σ_{N_lay}. Note that, in EM sounding problems, typically $\mathbf{Re}\,\sigma_0 \le 10^{-9}$.

The function $U_\gamma(z, z_*, \lambda)$ is defined as a unique solution of the problem

$$
\begin{cases}
\dfrac{\partial^2}{\partial z^2}U_\gamma(z,z_*,\lambda)-\eta_0^2U_\gamma(z,z_*,\lambda)=0, z<d_1, z\neq z_*,\\
\dfrac{\partial^2}{\partial z^2}U_\gamma(z,z_*,\lambda)-\eta_n^2U_\gamma(z,z_*,\lambda)=0, d_n<z<d_{n+1}, z\neq z_*,\\
\dfrac{\partial^2}{\partial z^2}U_\gamma(z,z_*,\lambda)-\eta_{N_{\text{lay}}}^2U_\gamma(z,z_*,\lambda)=0, z>d_{N_{\text{lay}}}, z\neq z_*,\\
\left[U_\gamma(z,z_*,\lambda)\right]_{z=d_n}=0,\\
\left[\dfrac{1}{\gamma}\dfrac{\partial}{\partial z}U_\gamma(z,z_*,\lambda)\right]_{z=d_n}=0,\\
\left[U_\gamma(z,z_*,\lambda)\right]_{z=z_*}=0,\\
\left[\dfrac{\partial}{\partial z}U_\gamma(z,z_*,\lambda)\right]_{z=z_*}=-2,\\
\left|U_\gamma(z,z_*,\lambda)\right|\to 0 \text{ as } z\to\pm\infty,\\
\eta_m^2=\lambda^2-k_m^2,\quad k_m^2=\mathrm{i}\omega\mu_0\sigma_m,\\
m=0\ldots N_{\text{lay}},\quad n=1\ldots N_{\text{lay}}-1,\quad 0<\lambda<\infty.
\end{cases}
\tag{28}
$$

The following procedure is performed to obtain an explicit expression for U_γ that allows analytical integration. Let $l_0=0, l_{N_{\text{lay}}}=0, l_n=d_{n+1}-d_n, n=1\ldots N_{\text{lay}}-1$. Define $p_m^\gamma, q_m^\gamma, m=0\ldots N_{\text{lay}}$ by the recurrent expressions

$$
\begin{aligned}
&p_0^\gamma=0; && q_{N_{\text{lay}}}^\gamma=0;\\
&p_1^\gamma=\frac{1-\alpha_0^\gamma\frac{\eta_0}{\eta_1}}{1+\alpha_0^\gamma\frac{\eta_0}{\eta_1}}; && q_{N_{\text{lay}}-1}^\gamma=\frac{1-\beta_{N_{\text{lay}}}^\gamma\frac{\eta_{N_{\text{lay}}}}{\eta_{N_{\text{lay}}-1}}}{1+\beta_{N_{\text{lay}}}^\gamma\frac{\eta_{N_{\text{lay}}}}{\eta_{N_{\text{lay}}-1}}};\\
&p_{m+1}^\gamma=\frac{1+\alpha_m^\gamma\frac{\eta_m}{\eta_{m+1}}\frac{p_m^\gamma\mathrm{e}^{-2\eta_m l_m}-1}{p_m^\gamma\mathrm{e}^{-2\eta_m l_m}+1}}{1-\alpha_m^\gamma\frac{\eta_m}{\eta_{m+1}}\frac{p_m^\gamma\mathrm{e}^{-2\eta_m l_m}-1}{p_m^\gamma\mathrm{e}^{-2\eta_m l_m}+1}}, && q_{m-1}^\gamma=\frac{1+\beta_m^\gamma\frac{\eta_m}{\eta_{m-1}}\frac{q_m^\gamma\mathrm{e}^{-2\eta_m l_m}-1}{q_m^\gamma\mathrm{e}^{-2\eta_m l_m}+1}}{1-\beta_m^\gamma\frac{\eta_m}{\eta_{m-1}}\frac{q_m^\gamma\mathrm{e}^{-2\eta_m l_m}-1}{q_m^\gamma\mathrm{e}^{-2\eta_m l_m}+1}},\\
&\quad m\neq N_{\text{lay}}; && \quad m\neq 0;\\
&\alpha_m^\gamma=\begin{cases}1, & \gamma=1;\\ \dfrac{\sigma_{m+1}}{\sigma_m}, & \gamma=\sigma;\end{cases} && \beta_m^\gamma=\begin{cases}1, & \gamma=1;\\ \dfrac{\sigma_{m-1}}{\sigma_m}, & \gamma=\sigma.\end{cases}
\end{aligned}
\tag{29}
$$

Let $d_0=d_1, d_{N_{lay+1}}=d_{N_{\text{lay}}}$ and let points z_r, z_s belong to layers r and s, respectively, $0\le r,s\le N_{\text{lay}}$. Then, using expressions (29), one gets

$$U_\gamma(z_r, z_s, \lambda) = \begin{cases} A^\gamma_{r,s}\left(p^\gamma_r \mathrm{e}^{2\eta_r d_r}\mathrm{e}^{-\eta_r z_r} + \mathrm{e}^{\eta_r z_r}\right)\left(\mathrm{e}^{-\eta_s z_s} + q^\gamma_s \mathrm{e}^{-2\eta_s d_{s+1}}\mathrm{e}^{\eta_s z_s}\right) \\ \qquad\qquad \text{for} \quad z_r \le z_s; \\ A^\gamma_{s,r}\left(p^\gamma_s \mathrm{e}^{2\eta_s d_s}\mathrm{e}^{-\eta_s z_s} + \mathrm{e}^{\eta_s z_s}\right)\left(\mathrm{e}^{-\eta_r z_r} + q^\gamma_r \mathrm{e}^{-2\eta_r d_{r+1}}\mathrm{e}^{\eta_r z_r}\right) \\ \qquad\qquad \text{for} \quad z_r > z_s, \end{cases} \tag{30}$$

where

$$\begin{aligned} A^\gamma_{r,s} &= Q^\gamma_r \times Q^\gamma_{r+1} \times \cdots \times Q^\gamma_{s-1} A^\gamma_{s,s}, \quad \text{for} \quad r < s, \\ Q^\gamma_m &= \frac{1 + p^\gamma_{m+1}}{1 + p^\gamma_m \mathrm{e}^{-2\eta_m l_m}} \mathrm{e}^{(\eta_{m+1} - \eta_m) d_{m+1}}, \quad \text{for} \quad m = 1 \ldots N_{\text{lay}} - 1, \\ A^\gamma_{n,n} &= \frac{1}{\eta_n\left(1 - p^\gamma_n q^\gamma_n \mathrm{e}^{-2\eta_n l_n}\right)}, \quad \text{for} \quad r = s = n, n = 0 \ldots N_{\text{lay}}, \\ A^1_{r,s} &= A^1_{s,r}, \quad A^\sigma_{r,s} = \frac{\sigma_r}{\sigma_s} A^\sigma_{s,r}, \quad \text{for} \quad r > s. \end{aligned} \tag{31}$$

To check Eq. (30), one can explicitly substitute Eq. (30) into Eq. (28), taking into account expressions (29) and (31).

In view of Eq. (30), one can see that integrals in formulas (27) (i.e., the integrals over $U_\gamma(z, z_*, \lambda)$ and its partial derivatives) can be obtained analytically with respect to z, z_* over any domains that do not intersect the layer boundaries. However, rounding errors arising in addition and multiplication of very small or large quantities make the formula (30) impractical for $\lambda \gg 1$. Instead, the following formula is used:

$$U_\gamma(z_r, z_s, \lambda) = \begin{cases} A^\gamma_{r,s}\Big(p^\gamma_r \mathrm{e}^{-(\eta_r z_r + \eta_s z_s - 2\eta_r d_r)} + q^\gamma_s \mathrm{e}^{-(2\eta_s d_{s+1} - (\eta_r z_r + \eta_s z_s))} + \\ \quad \mathrm{e}^{-(\eta_s z_s - \eta_r z_r)} + p^\gamma_r q^\gamma_s \mathrm{e}^{-(2(\eta_s d_{s+1} - \eta_r d_r) - (\eta_s z_s - \eta_r z_r))}\Big) \\ \qquad\qquad \text{for} \quad z_r \le z_s; \\ A^\gamma_{s,r}\Big(p^\gamma_s \mathrm{e}^{-(\eta_s z_s + \eta_r z_r - 2\eta_s d_s)} + q^\gamma_r \mathrm{e}^{-(2\eta_r d_{r+1} - (\eta_s z_s + \eta_r z_r))} + \\ \quad \mathrm{e}^{-(\eta_r z_r - \eta_s z_s)} + p^\gamma_s q^\gamma_r \mathrm{e}^{-(2(\eta_r d_{r+1} - \eta_s d_s) - (\eta_r z_r - \eta_s z_s))}\Big) \\ \qquad\qquad \text{for} \quad z_r > z_s. \end{cases} \tag{32}$$

Formula (32) overcomes the aforementioned problem, since the real parts of all the exponents' powers are negative. The consequent calculations provide accurate and robust results for any $0 < \lambda < \infty$.

Consider N_z subdomains in the discretization in vertical direction. To obtain the matrix $\widehat{B}^m_n$ for the system (15), one needs to compute $O\left(N_z^2\right)$ complex exponents in Eq. (32). An algorithm requiring only $O\left(N_z\right)$ complex exponent calculations has been developed to speed up this integration procedure.

Let $z_0 < z_1 < \cdots < z_{N_z}$. Suppose that the intervals $[z_l, z_{l+1}]$, $l = 0 \ldots N_z - 1$ do not intersect the layers' boundaries. For $i, j = 0 \ldots N_z - 1$, $0 \le \alpha + \beta \le 2$, one needs to calculate $W^{\alpha,\beta}_{i,j}(\gamma) = \int_{z_i}^{z_{i+1}} \frac{\partial^\alpha}{\partial z^\alpha}\left(\int_{z_j}^{z_{j+1}} \left[\frac{\partial^\beta}{\partial z_*^\beta} U_\gamma(z, z_*, \lambda)\right] \mathrm{d}z_*\right) \mathrm{d}z$.

Let r_l be an index of the layer containing $[z_l, z_{l+1}]$, $l = 0 \ldots N_z - 1$. Then, using Eq. (30), one obtains for $z_i < z_j$

$$W_{i,j}^{\alpha,\beta}(\gamma) = \int_{z_i}^{z_{i+1}} \left(\frac{\partial^\alpha}{\partial z^\alpha} \int_{z_j}^{z_{j+1}} \left[\frac{\partial^\beta}{\partial z_*^\beta} U_\gamma(z, z_*, \lambda) \right] \mathrm{d}z_* \right) \mathrm{d}z = H_\gamma^\alpha(z_i, z_{i+1}) \prod_{l=i+1}^{l=j} \Theta_l^\gamma \int_{z_j}^{z_{j+1}} \left(\frac{\partial^\beta}{\partial z_*^\beta} U\gamma(z_j, z_*, \lambda) \right) \mathrm{d}z_*, \tag{33}$$

where

$$H_\gamma^\alpha(z_i, z_{i+1}) = \frac{\int_{z_i}^{z_{i+1}} \left(\frac{\partial^\alpha}{\partial z^\alpha} \left[p_{r_i}^\gamma \mathrm{e}^{-\eta_{r_i}(z+z_{i+1}-2d_{r_i})} + \mathrm{e}^{-\eta_{r_i}(z_{i+1}-z)} \right] \right) \mathrm{d}z}{p_{r_i}^\gamma \mathrm{e}^{-2\eta_{r_i}(z_{i+1}-d_{r_i})} + 1},$$

$$\Theta_l^\gamma = \varkappa_l^\gamma \frac{p_{r_l}^\gamma \mathrm{e}^{-\eta_{r_l}((z_l+z_{l+1})-2d_{r_l})} + \mathrm{e}^{-\eta_{r_l}(z_{l+1}-z_l)}}{p_{r_l}^\gamma \mathrm{e}^{2\eta_{r_l}(d_{r_l}-z_{l+1})} + 1}, \tag{34}$$

$$\varkappa_l^\gamma = \left\{ \begin{array}{ll} 1, & r_l = r_{l+1} \\ Q_{r_{l+1}}^\gamma, & r_l \neq r_{l+1} \end{array} \right\}.$$

All the exponents in Eq. (34) vanish as $\lambda \to \infty$, so the corresponding computations do not depend on round-off errors due to machine precision. The formulas for $z_i > z_j$ are similar. The integrals $W_{ii}^{\alpha,\beta}$ are computed analytically using formulas (32). Since Θ_l^γ depends only on $l = 1 \ldots N_z$ and $\gamma = 1, \sigma$, one only needs to calculate $O(N_z)$ complex exponents using factorization from expressions (33), (34).

Appendix C: Horizontal Integration

The integrals (26) are a particular case of the integral

$$I_{\alpha,\beta} = \int_{S_n} \frac{\partial^{\alpha+\beta}}{\partial x^\alpha \partial y^\beta} \left\{ \int_{S_m} \left[\int_0^\infty J_0(\rho\lambda) f(\lambda) \mathrm{d}\lambda \right] \mathrm{d}S_m \right\} \mathrm{d}S_n, \tag{35}$$
$$\rho = \sqrt{(x - x_0)^2 + (y - y_0)^2}, \quad 0 \leq \alpha + \beta \leq 2,$$

where $f(\lambda)$ is some easily computed function, and $S_n = [x_n, x_n + h_x] \times [y_n, y_n + h_y]$, $S_m = [x_m, x_m + h_x] \times [y_m, y_m + h_y]$ are rectangular domains with similar sizes.

The key feature of the proposed method is transformation of the integrals (35) to one-dimensional convolution integrals. Taking for simplicity $\alpha = \beta = 0$, one has

$$
\begin{aligned}
I_{0,0} = F(R;\, p, q, \varphi) &= \int_0^{\infty} K(R\lambda;\, p, q, \varphi) f(\lambda) \frac{\mathrm{d}\lambda}{\lambda^4}, \\
K(R\lambda;\, p, q, \varphi) &= \lambda^4 \int_{S_m} \int_{S_n} J_0(\rho\lambda) \mathrm{d}S_m \mathrm{d}S_n \\
&= \lambda^4 \int_{x_n}^{x_n+h_x} \int_{y_n}^{y_n+h_y} \int_{x_m}^{x_m+h_x} \int_{y_m}^{y_m+h_y} J_0(\rho\lambda) \mathrm{d}x_0 \mathrm{d}y_0 \mathrm{d}x \mathrm{d}y \\
&= \int_0^{R\lambda p} \int_0^{R\lambda q} \int_{R\lambda\left(\cos\varphi - \frac{p}{2}\right)}^{R\lambda\left(\cos\varphi + \frac{p}{2}\right)} \int_{R\lambda\left(\sin\varphi - \frac{q}{2}\right)}^{R\lambda\left(\sin\varphi + \frac{q}{2}\right)} J_0(\tau) d\tilde{x} d\tilde{x}_0 d\tilde{y} d\tilde{y}_0, \qquad (36)
\end{aligned}
$$

where

$$
\begin{aligned}
\tau &= \sqrt{(\tilde{x} - \tilde{x}_0)^2 + (\tilde{y} - \tilde{y}_0)^2}; \\
R &= \sqrt{\left(x_n - x_m - \frac{h_x}{2}\right)^2 + \left(y_n - y_m - \frac{h_y}{2}\right)^2}; \\
p &= \frac{h_x}{R} \quad q = \frac{h_y}{R} \quad \varphi = \arctan \frac{y_n - y_m - \frac{h_y}{2}}{x_n - x_m - \frac{h_x}{2}}.
\end{aligned}
$$

Let $\lambda = \mathrm{e}^{-t}$, $R = \mathrm{e}^{s}$

$$
\begin{aligned}
F\left(\mathrm{e}^{s};\, p, q, \varphi\right) &= \mathrm{e}^{3s} \int_{-\infty}^{\infty} \Phi(s - t;\, p, q, \varphi) f\left(\mathrm{e}^{-t}\right) \mathrm{d}t, \\
\Phi(s - t;\, p, q, \varphi) &= K\left(\mathrm{e}^{s-t};\, p, q, \varphi\right) \mathrm{e}^{-3(s-t)}.
\end{aligned} \qquad (37)
$$

For fixed p, q, φ the integral in Eq. (37) is the convolution integral with kernel Φ. Note that, for different values of α and β, the kernels can be obtained similarly.

The main advantage of using the convolution integrals is that their computation does not require explicit calculation of the kernel Φ. Consider the input function $v(t)$ and the output function $u(s)$ such that

$$
u(s) = \int_{-\infty}^{+\infty} \Phi(s - t) v(t) \mathrm{d}t. \qquad (38)
$$

For some $N = 2M, l, 0 < \xi < 0.5l, k = -M \ldots M-1$, define

$$W_s = (-1)^s \frac{1}{N} \sum_{n=-M}^{M-1} \left\{ \frac{\sum_{m=-M}^{M-1} (-1)^m u(ml-\xi) \mathrm{e}^{-2\mathrm{i}\pi \frac{mn}{N}}}{\sum_{m=-M}^{M-1} (-1)^m v(ml+0.5l) \mathrm{e}^{-2\mathrm{i}\pi \frac{mn}{N}}} \right\} \mathrm{e}^{2\mathrm{i}\pi \frac{sn}{N}}. \tag{39}$$

Then, for any $g(t)$, one gets

$$\int_{-\infty}^{+\infty} \Phi(s-t) g(t) \mathrm{d}t \approx \sum_{s=N_1}^{N_2} W_s g(sl+\xi), \quad -M \le N_1 < N_2 \le M-1. \tag{40}$$

The tradeoff between the accuracy of approximation (40) and the computational time is achieved by the particular selection of M, N_1, N_2, l, ξ and functions u and v.

From Eqs. (36) and (40), the approximation formulas for integral (35) can be obtained as

$$\begin{aligned} I_{\alpha,\beta} &\approx R^{(3-\alpha-\beta)} \sum_{m=N_1}^{m=N_2} W_m^{\alpha,\beta}(p,q,\varphi,\alpha,\beta) f\left(\frac{\lambda_m}{R}\right), \\ \lambda_m &= \mathrm{e}^{ml+\xi}. \end{aligned} \tag{41}$$

For the given input function $v(t) = 8\mathrm{e}^{-t^2}\left(t^5 - 4t^3 + 2t\right)$, the output functions for different kernels can be expressed analytically by Gaussian and error functions. Inspired by (Anderson 1979), the parameters used are $l = 0.2, \xi = 0.0964, M = 512$, $N_1 = -250$, $N_2 = 200$. In computational experiments, these parameters provided appropriate accuracy in calculation of $\widehat{B}_n^m$.

References

Anderson W (1979) Numerical integration of related hankel transforms of order 0 and 1 by adaptive digital filtering. Geophysics 44:1287–1305

Avdeev D, Knizhnik S (2009) 3D integral equation modeling with a linear dependence on dimensions. Geophysics 74:89–94

Avdeev D, Kuvshinov A, Pankratov O, Newman G (2002) Three-dimensional induction logging problems, part I: an integral equation solution and model comparisons. Geophysics 67(2):413–426

Avdeev DB, Kuvshinov AV, Pankratov OV, Newman GA (1997) High-performance three-dimensional electromagnetic modelling using modified Neumann series. Wide-band numerical solution and examples. J Geomagn Geoelectr 49:1519–1539

Chave A, Jones A (2012) The magnetotelluric method: theory and practice. Cambridge University Press, Cambridge

Delves LM, Mohamed JL (1985) Computational methods for integral equations. Cambridge University Press, Cambridge

Dmitriev V, Silkin A, Farzan R (2002) Tensor Green function for the system of Maxwell's equations in a layered medium. Comput Math Model 13(2):107–118

Egbert GD, Kelbert A (2012) Computational recipes for electromagnetic inverse problems. Geophys J Int 189(1):251–267. doi:10.1111/j.1365-246X.2011.05347.x

Ernst O, Gander M (2012) Why it is difficult to solve helmholtz problems with classical iterative methods. In: Graham IG, Hou TY, Lakkis O, Scheichl R (eds) Numerical analysis of multiscale problems, lecture notes in computational science and engineering, vol 83. Springer, Berlin, pp 325–363

Farquharson CG, Miensopust MP (2011) Three-dimensional finite-element modelling of magnetotelluric data with a divergence correction. J Appl Geophys 75:699–710
Fraysse V, Giraud L, Gratton S, Langou J (2003) A set of GMRES routines for real and complex arithmetics on high performance computers. http://www.cerfacs.fr/algor/reports/2003/TR_PA_03_03.pdf
Frigo M, Johnson SG (2005) The design and implementation of FFTW3. Proc IEEE 93(2):216–231 (special issue on "Program Generation, Optimization, and Platform Adaptation")
Grayver A, Kolev T (2015) Large-scale 3D geo-electromagnetic modeling using parallel adaptive high-order finite element method. Geophysics 80(6):277–291
Haber E, Ascher UM (2001) Fast finite volume simulation of 3D electromagnetic problems with highly discontinuous coefficients. SIAM J Sci Comput 22(6):1943–1961
Hursan G, Zhdanov MS (2002) Contraction integral equation method in three-dimensional electromagnetic modeling. Radio Sci 37(6):1–13. doi:10.1029/2001RS002513
Jaysaval P, Shantsev DV, de la Kethulle de Ryhove S (2015) Efficient 3-D controlled-source electromagnetic modelling using an exponential finite-difference method. Geophys J Int 203(3):1541–1574. doi:10.1093/gji/ggv377
Kamm J, Pedersen LB (2014) Inversion of airborne tensor VLF data using integral equations. Geophys J Int 198(2):775–794. doi:10.1093/gji/ggu161
Koyama T, Utada H, Avdeev D (2008) Fast and memory-saved 3-D forward modeling code for MT by using integral equation method. In: Abstract book, 19th workshop on electromagnetic induction in the Earth, China
Kruglyakov M (2011) Modified integral current methods in electrodynamics of nonhomogeneous media. Comput Math Model 22(3):246–254
Kruglyakov M, Geraskin A, Kuvshinov A (2016) Novel accurate and scalable 3-D MT forward solver based on a contracting integral equation method. Comput Geosci 96:208–217. doi:10.1016/j.cageo.2016.08.017, http://www.sciencedirect.com/science/article/pii/S009830041630293X
Kruglyakov M, Geraskin A, Kuvshinov A (2016b) Novel scalable 3-D MT inverse solver (extrEMeI). In: Abstract GP51A-1357 presented at 2016 Fall meeting, AGU, San Francisco, Calif. 12–16 December, AGU, San Francisco
Mackie R, Smith J, Madden T (1994) 3-Dimensional electromagnetic modeling using finite-difference equation—the magnetotelluric example. Radio Sci 29(4):923–935
Mulder W (2006) A multigrid solver for 3D electromagnetic diffusion. Geophys Prospect 54:633–649
Newman G, Alumbaugh D (2002) Three-dimensional induction logging problems, part 2: a finite-difference solution. Geophysics 61:484–491
Pankratov O, Kuvshinov A (2016) Applied mathematics in EM studies with special emphasis on an uncertainty quantification and 3-D integral equation modelling. Surv Geophys 37(1):109–147. doi:10.1007/s10712-015-9340-4
Pankratov O, Avdeyev D, Kuvshinov A (1995) Electromagnetic-field scattering in a heterogeneous earth: a solution to the forward problem. Izv Phys Solid Earth 31(3):201–209
Puzyrev V, Koldan J, de la Puente J, Houzeaux G, Vazquez M, Cela JM (2013) A parallel finite-element method for three-dimensional controlled-source electromagnetic forward modelling. Geophys J Int 193:678–693
Raiche AP (1974) An integral equation approach to three-dimensional modelling. Geophys J Int 36(2):363–376
Ren Z, Kalscheuer T, Maurer Greenhalgh H S (2013) A goal-oriented adaptive finite-element approach for plane wave 3-D electromagnetic modelling. Geophys J Int 194:700–718
Saad Y (1993) A flexible inner-outer preconditioned GMRES algorithm. SIAM J Sci Comput 14(2):461–469
Sadovnichy V, Tikhonravov A, Voevodin V, Opanasenko V (2013) "Lomonosov": Supercomputing at Moscow State University. In: Vetter JS (ed) Contemporary high performance computing: from petascale toward exascale. Chapman & Hall/CRC Computational Science, Boca Raton, pp 283–307
Schwarzbach C, Börner RU, Spitzer K (2011) Three-dimensional adaptive higher order finite element simulation for geo-electromagnetics—a marine CSEM example. Geophys J Int 187:63–74
Singer B (1995) Method for solution of Maxwell's equations in non-uniform media. Geophys J Int 120:590–598
Singer B (2008) Electromagnetic integral equation approach based on contraction operator and solution optimization in Krylov subspace. Geophys J Int 175:857–884
Sun J, Kuvshinov A (2015) Accelerating EM integral equation forward solver for global geomagnetic induction using SVD based matrix compression method. Geophys J Int 200(2):1005–1011

Varentsov IM, Fomenko IY, Golubev NG, Mehanee S, Hursan G, Zhdanov MS (2000) Comparative study of 3-D finite difference and integral equation methods. In: Proceedings of 2000 consortium for electromagnetic modeling and inversion annual meeting. University of Utah, Salt Lake City, pp 35–74

Wang Q, Zhang X, Zhang Y, Yi Q (2013) AUGEM: automatically generate high performance dense linear algebra kernels on x86 CPUs. In: International conference for high performance computing, networking, storage and analysis, SC'13, Denver, CO, USA, pp 1–12. http://www.openblas.net

Wannmaker PE (1991) Advances in three-dimensional magnetotelluric modeling using integral equations. Geophysics 56:1716–1728

Ward SH, Hohmann GW (1988) 4. Electromagnetic theory for geophysical applications, SEG,USA, chap 4, pp 130–311

Weidelt P (1975) Electromagnetic induction in three-dimensional structures. J Geophys-Z Geophys 41:85–109